Chinese Journal of Structural Chemistry

ARTICLE

Engineering the Interface and Interaction Structure on Highly Coke-Resistant Ni/CeO_2-Al_2O_3 Catalyst for Dry Reforming of Methane

Sha Li[1], Xin Wang[1], Min Cao[1], Jingjun Lu[1], Li Qiu[1] and Xiaoliang Yan[1,2]*

[1]*College of Chemical Engineering and Technology, Taiyuan University of Technology, Taiyuan 030024, China*

[2]*State Key Laboratory of Clean and Efficient Coal Utilization, Taiyuan University of Technology, Taiyuan 030024, China*

ABSTRACT Designing and tailoring metal-support interaction in Ni-based catalysts with plentiful interfacial sites is of significant interest for achieving a targeted catalytic performance in dry reforming of methane (DRM), but remains as a challenging task. In this work, Ni/Al_2O_3 and Ni/CeO_2-Al_2O_3 catalysts with the same strong metal-support interaction (SMSI) but distinct interface structure are developed by an improved evaporation-induced self-assembly method using pseudobohemite gel as aluminum source. Ni/CeO_2-Al_2O_3 exhibits superior catalytic activity and stability in DRM in comparison with Ni/Al_2O_3. The highest CH_4 and CO_2 conversion reaches at 71.4% and 82.1% for Ni/CeO_2-Al_2O_3, which are higher than that of 64.3% and 75.6% for Ni/Al_2O_3 at 700 °C. The SMSI effect in Ni/CeO_2-Al_2O_3 provides more active interfacial sites with less coke deposition, and promotes the generation of active formate species which are the key intermediates for DRM. The findings of the present work could possibly pave the way for fabricating catalysts with SMSI strategy for efficient heterogeneous catalysis.

Keywords: metal-support interaction, interface, Ni catalysts, CeO_2, dry reforming of methane

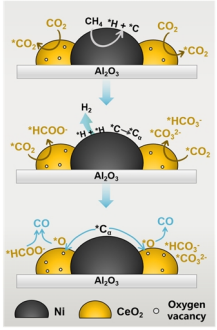

n INTRODUCTION

Dry reforming of methane (DRM) has been well regarded as a promising process for the effective conversion of two greenhouse gases (CH_4 and CO_2) into synthesis gas (CO and H_2), which can be used as a versatile feedstock for value-added chemicals and fuels.[1-4] Among various applied catalysts, Ni-based catalysts with comparable activity as noble-based catalysts have been designed and developed for highly efficient DRM.[5-8] However, owing to the endothermic feature of DRM, the reaction is thermodynamically favorable at high temperature, where sintering of Ni particles easily occurs and causes the decline of the catalytic performance. Furthermore, coke deposition by the presence of large amounts of carbon filaments from CH_4 and CO dissociation is the main origin for the deactivation of the catalysts.

A potential solution to the sintering and coking issues is to modify the structures of Ni-based catalysts by building strong metal-support interaction (SMSI) with plentiful interfacial sites for the reaction.[9-12] Among them, industrially and widely used Al_2O_3 support Ni catalysts have gained much attention. SMSI effect on Ni/Al_2O_3 facilitated the generation of small and homogeneous Ni particles on Al_2O_3 support as originated from the formation of active $NiAl_2O_4$ spinel.[13] However, if the metal-support interaction on Ni/Al_2O_3 is too strong, inactive $NiAl_2O_4$ spinel would be produced, which would be difficult to reduce to Ni particles at a moderate temperature and high temperature reduction from $NiAl_2O_4$ to Ni particles would result in the growth of large Ni particles.[14,15]

Generally, introducing CeO_2 into Ni/Al_2O_3 with the formation of Ni/CeO_2-Al_2O_3 is able to improve Ni reducibility at low temperature with a high dispersion of Ni particles, owing to the fact that CeO_2 exhibits remarkable oxygen mobility and excellent redox properties (Ce^{4+}/Ce^{3+}).[16,17] The SMSI effect between metal and support in Ni/CeO_2-Al_2O_3 catalysts provides fruitful benefits and enhancements towards heterogeneous catalysis, including in steam or dry reforming of methane, catalytic biomass gasification, CO_2 methanation, reverse water-gas shift and methane catalytic decomposition.[18-22] Specifically, the addition of CeO_2 in Ni/Al_2O_3 is able to change the metal-support interaction with different reductive behaviors, which plays an important role in controlling particle size, tuning electronic structure of Ni, providing oxygen species and stabilizing active phase of Al_2O_3.[20-22] However, the changes of interaction and interface structures in Ni/CeO_2-Al_2O_3 usually occur simultaneously. Therefore, it is critical to investigate the accurate role of interaction or interface in Ni/CeO_2-Al_2O_3 to boost catalytic performance.

In this work, two strategies of interpreting the effects of SMSI and interface in Ni/CeO_2-Al_2O_3 on catalytic performance were proposed. One involved manipulating the same metal-support interaction with different interface structures by comparing Ni/CeO_2-Al_2O_3 with Ni/Al_2O_3, and the other included controlling the same interface structure but different interaction of two Ni/CeO_2-Al_2O_3 catalysts. Specifically, pseudobohemite (AlOOH), being extensively used as binder and alumina precursor in industry, was first treated with nitric acid under microwave irradiation to generate aluminum gel. Afterwards, the obtained gel, rather than aluminum isopropoxide as a classic aluminium source, was blended with the solution of Ni^{2+} and/or Ce^{3+} ions and placed on a Petri dish for a modified evaporation-induced self-assembly (mEISA) method.[23] The resultant Ni/CeO_2-Al_2O_3 catalyst presented porous structure with a high surface area, and most importantly, the SMSI effect on Ni/CeO_2-Al_2O_3 with tailored interface in Ni-CeO_2 promoted the catalytic activity and stability in DRM with enhanced resistance of coke deposition and sintering of Ni particles.

n RESULTS

Characterizations of NiO/Al_2O_3 and NiO/CeO_2-Al_2O_3. Aluminum gel with white translucent feature was originally generated from industrial pseudo-bohemite (AlOOH) by nitric acid treatment

DOI: 10.14102/j.cnki.0254-5861.2022-0113

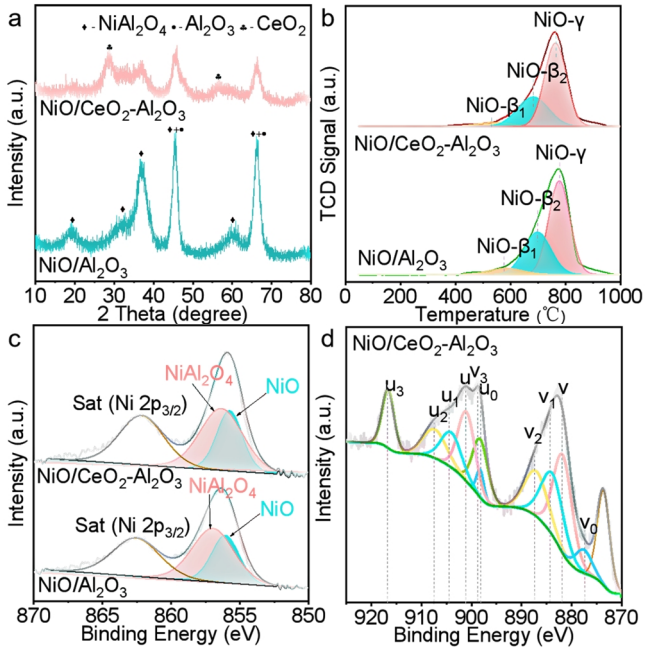

Figure 1. (a) XRD patterns, (b) H_2-TPR profiles and (c, d) Ni 2p and Ce 3d XPS spectra of NiO/Al_2O_3 and NiO/CeO_2-Al_2O_3.

under microwave irradiation for 1 h. The gel was then fully mixed with ethanol solution containing Ni^{2+} and/or Ce^{3+} ions. The solution in the mixture was evaporated in an oven and the fresh samples were produced by thermal calcination of the dried mixture at 600 °C under air. The resultant samples, including NiO/Al_2O_3 and NiO/CeO_2-Al_2O_3, exhibit light blue and bluish-green colors, respectively. Ni content is 8.9% for the former and 9.1% for the latter, separately, and Ce loading is 9.6% for NiO/CeO_2-Al_2O_3 according to the results of inductively coupled-plasma atomic emission spectroscopy (ICP-AES) measurements. NiO/Al_2O_3 and NiO/CeO_2-Al_2O_3 possessed large BET surface areas of 171 and 197 $m^2\ g^{-1}$, respectively, and have similar pore diameter distribution of approximate 16 nm (Table S1 and Figure S1).

The powder X-ray diffraction (PXRD) patterns of NiO/Al_2O_3 and NiO/CeO_2-Al_2O_3 are shown in Figure 1a. Both samples show characteristic diffraction peaks for Al_2O_3 (circle mark) and $NiAl_2O_4$ (diamond mark). Besides, two peaks indexed to (111) and (311) planes for CeO_2 (star mark) appeared on NiO/CeO_2-Al_2O_3. The reductive behaviors of NiO/Al_2O_3 and NiO/CeO_2-Al_2O_3 were studied by temperature programmed reduction with H_2 (H_2-TPR), as shown in Figure 1b. Three deconvoluted peaks can be detected at 550, 680, and 750 °C on the two samples. The high temperature peak originated from the reduction of crystalline spinel (NiO-γ) and the first two peaks corresponded to the formation of NiO (NiO-β1 and NiO-β2) considerably interacted with support.[24,25] The ratio of NiO-β1:NiO-β2:NiO-γ was 6.1:34.4:59.5 for NiO/Al_2O_3 and 4.8:32.0:63.2 for NiO/CeO_2-Al_2O_3, respectively, which indicates that the two samples possessed the same metal-support interaction with 40% of NiO-β species. Compared with previous work,[16,17] the addition of CeO_2 into NiO/Al_2O_3 hardly affected the reductive behaviors of NiO/CeO_2-Al_2O_3, which was probably owing to the different method and low CeO_2 loading content in this work.

Figure 1c shows the X-ray photoelectron spectra for Ni $2p_{3/2}$ on NiO/Al_2O_3 and NiO/CeO_2-Al_2O_3. Two peaks of nickel in +2 state exist, which are attributed to the presence of NiO and $NiAl_2O_4$ on the surface of both samples.[26,27] Therefore, the two samples possess strong metal-support interaction between Ni and support as well as similar surface amount of NiO (37.1% for NiO/Al_2O_3 and 38.8% for NiO/CeO_2-Al_2O_3) and $NiAl_2O_4$ (62.9% for NiO/Al_2O_3 and 61.2% for NiO/CeO_2-Al_2O_3). In addition, the XPS spectrum of Ce 3d of NiO/CeO_2-Al_2O_3 presents the generation of Ce^{3+} and Ce^{4+} species, where the former accounted about 32% of the total amount of surface cerium.

Characterizations of Ni/Al_2O_3 and Ni/CeO_2-Al_2O_3 Catalysts. NiO/Al_2O_3 and NiO/CeO_2-Al_2O_3 were reduced at 550 °C under H_2 flow to generate Ni/Al_2O_3 and Ni/CeO_2-Al_2O_3 catalysts, respectively. Because the Ni characteristic diffraction peaks of XRD patterns for reduced catalysts are not apparent, H_2 pulse chemisorption was carried out to characterize the accessible nickel on the catalysts (Table S2). Both catalysts have similar active Ni surface area of 55 $m^2\ g^{-1}$ with Ni dispersion of 6.5%, and the particle sizes of Ni particles were calculated to be 7.8 nm for Ni/Al_2O_3 and 6.5 nm for Ni/CeO_2-Al_2O_3, respectively.

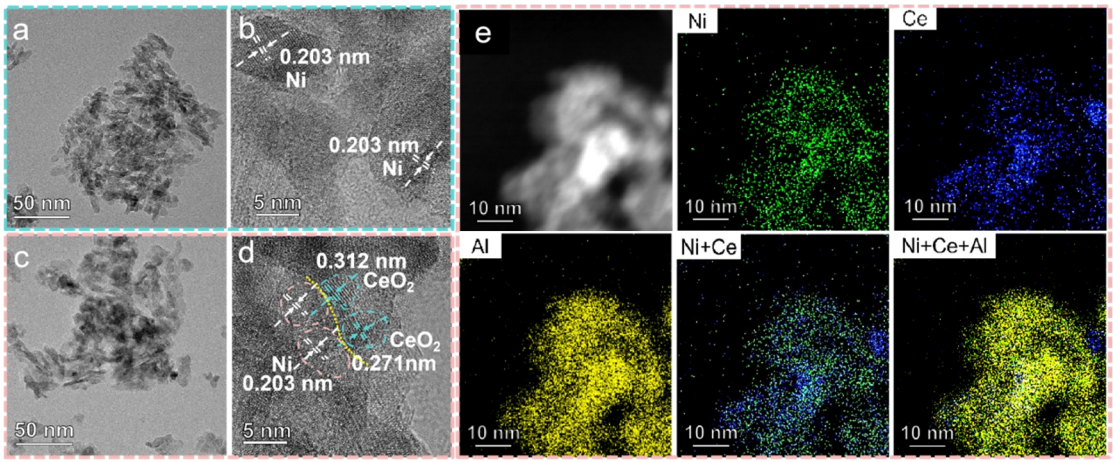

Figure 2. TEM images of (a, b) Ni/Al_2O_3 and (c, d) Ni/CeO_2-Al_2O_3. (e) HADDF STEM-EDX mapping of Ni/CeO_2-Al_2O_3.

Chin. J. Struct. Chem. **2022**, 41, 2212007-2212014
DOI: 10.14102/j.cnki.0254-5861.2022-0113

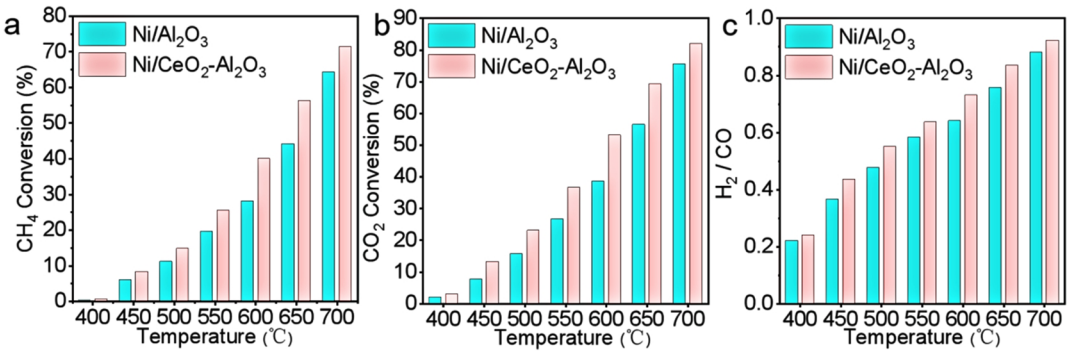

Figure 3. (a) CH_4 and (b) CO_2 conversion as well as (c) H_2/CO ratio on Ni/Al_2O_3 and Ni/CeO_2-Al_2O_3 in DRM.

The morphological observation of Ni/Al_2O_3 and Ni/CeO_2-Al_2O_3 was studied by transmission electron microscope (TEM) measurements, as shown in Figure 2. Both catalysts showed rod-like structure with the length of about 30 nm and width of 10 nm (Figure 2a and c). No aggregation of Ni particles can be observed on the two catalysts. The dominantly exposed plane of Ni/Al_2O_3 and Ni/CeO_2-Al_2O_3 presented the lattice spacing of 0.203 nm, which originated to the (111) plane of Ni (Figure 2b and d). Furthermore, Ni/CeO_2-Al_2O_3 exhibited lattice spacing of 0.312 and 0.271 nm, corresponding to the (111) and (200) planes of CeO_2. It should be noted that Ni particles were closely interacted and intimately contacted with CeO_2, leading to the formation of interface structure between metal and support. This can be further illustrated by energy-dispersive X-ray (EDX) mapping analysis in Figure 2e, where green nickel element finely scattered between the blue cerium element and homogeneously dispersed in the yellow aluminum element.

Catalytic Performances of Ni/Al_2O_3 and Ni/CeO_2-Al_2O_3 in DRM Reaction. The catalytic performances of Ni/Al_2O_3 and Ni/CeO_2-Al_2O_3 for DRM reaction were carried out from 400 to 700 °C under a GHSV of 24000 mL g^{-1} h^{-1} with a CH_4:CO_2 feed ratio of 1:1. As shown in Figure 3a and b, the conversion of CO_2 is higher than that of CH_4 under the same temperature, owing to the occurrence of reverse water gas shift (RWGS) reaction. For the catalytic behavior, Ni/CeO_2-Al_2O_3 exhibits superior activity compared to Ni/Al_2O_3 in the whole temperature region. For instance, the highest CH_4 and CO_2 conversion is 71.4% and 82.1% on Ni/CeO_2-Al_2O_3, respectively, which is higher than 64.3% and 75.6% on Ni/Al_2O_3 at 700 °C. Meanwhile, H_2/CO ratio reaches 0.88 and 0.92 on Ni/Al_2O_3 and Ni/CeO_2-Al_2O_3 at 700 °C, respectively. The higher H_2/CO ratio suggests the less favorability for RWGS reaction on the latter in comparison to the former. Therefore, the addition of CeO_2 to Ni/Al_2O_3 obviously promoted the catalytic performances in DRM reaction.

Stability Investigation of Ni/Al_2O_3 and Ni/CeO_2-Al_2O_3 in DRM Reaction. The long-term activities of Ni/Al_2O_3 and Ni/CeO_2-Al_2O_3 catalysts were studied and the time on stream of conversions for CH_4 and CO_2 on the two catalysts during DRM at 500 °C is shown in Figure 4a and b. CH_4 conversion of Ni/Al_2O_3 dramatically declined from 11.7% to 6.1% during the whole test of period (Figure 4a). Meanwhile, CO_2 conversion of Ni/Al_2O_3 decreased from 16.2% to 9.2% with 30 h on stream (Figure 4b). Ni/CeO_2-Al_2O_3 exhibited distinct behaviors and CH_4 conversion mainly stabilized at 12.1% up to 50 h with only a slight decline in the first 5 h. CO_2 conversion of the catalyst slightly decreased at the first 5 h and reached a stable value of 16.1% with 50 h on stream. The time dependent H_2/CO ratios of Ni/Al_2O_3 and Ni/CeO_2-Al_2O_3 are presented in Figure 4c. H_2/CO ratio of Ni/Al_2O_3 dropped consistently during the stability test; whereas the ratio of Ni/CeO_2-Al_2O_3 decreased firstly and finally stabilized to around 0.35 after 40 h. Therefore, Ni/CeO_2-Al_2O_3 possessed higher catalytic long-term stability than Ni/Al_2O_3.

Characterizations of the Used Catalysts after Stability Test. The used Ni/Al_2O_3 and Ni/CeO_2-Al_2O_3 after stability test were characterized by O_2-TPO measurement to determine the structure of carbonaceous species (Figure 5). It has been widely accepted that the deposited carbon species on Ni catalysts could

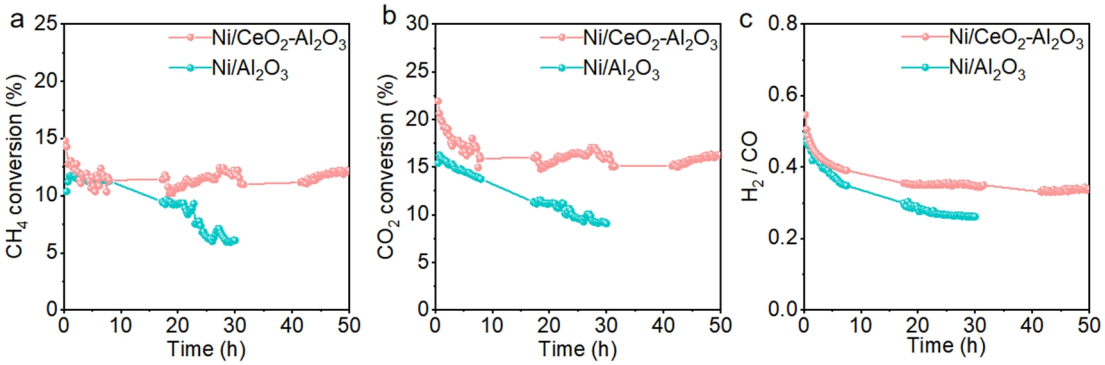

Figure 4. Stability test of Ni/Al_2O_3 and Ni/CeO_2-Al_2O_3 in DRM at 500 °C.

DOI: 10.14102/j.cnki.0254-5861.2022-0113

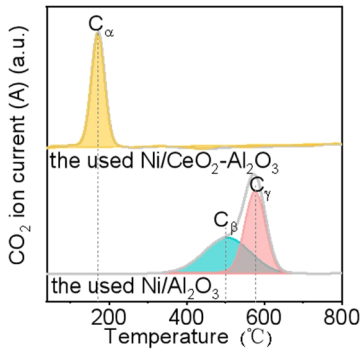

Figure 5. O_2-TPO profiles of the used Ni/Al_2O_3 and Ni/CeO_2-Al_2O_3 after stability test.

be classified into three types, active carbon atom (C_α), less active (C_β) and inactive coke (C_γ), on the basis of burning-off temperature.[28-30] Active C_α species were generated on the used Ni/CeO_2-Al_2O_3, as evidenced by the presence of oxidation peak at 170 °C on the O_2-TPO curve, which was the origin for the efficient and stable catalytic behavior. However, only C_β and C_γ species existed on the used Ni/Al_2O_3, which was confirmed by the high oxidation peaks at the temperature of 470 and 580 °C on the O_2-TPO curve, thus resulting in the loss of catalytic performance. The amounts of deposited carbon on the two used catalysts were further determined by automatic carbon element analyzer. The accurate amounts of carbon deposition on the used Ni/Al_2O_3 and Ni/CeO_2-Al_2O_3 are 1.25% and 0.85%, respectively. The coke deposition rate on the latter (0.42 $mg_c\ g_{cat}^{-1}\ h^{-1}$) is slower than that on the former (0.17 $mg_c\ g_{cat}^{-1}\ h^{-1}$). Based on XPS result, the redox cycles (Ce^{4+}/Ce^{3+}) are associated with the presence of oxygen vacancies on Ni/CeO_2-Al_2O_3, which is beneficial for the removal of carbonaceous species during DRM.

To digger deeply into the morphological structure of the deposited carbon species, TEM measurements were further conducted and the results are illustrated in Figure 6. No obvious carbon filaments were observed on the used catalysts in Figure 6a and c by low resolution TEM analyses. However, encapsulated carbon, as carbon onion spheres, with Ni NPs inside existed on the used Ni/Al_2O_3 (Figure 6b). The graphitic carbon hardly presented on the used Ni/CeO_2-Al_2O_3 by careful detection (Figure 6d). Moreover, the formation and existence of interface structure between Ni and CeO_2 can be clearly seen, indicating the stable interface structure on Ni/CeO_2-Al_2O_3, which is originated from the SMSI effect, as shown from the H_2-TPR and TEM analyses. Meanwhile, this SMSI on Ni/CeO_2-Al_2O_3 well restricted the growth of Ni particles, as evidenced by the homogeneous Ni particles in Figure 6c.

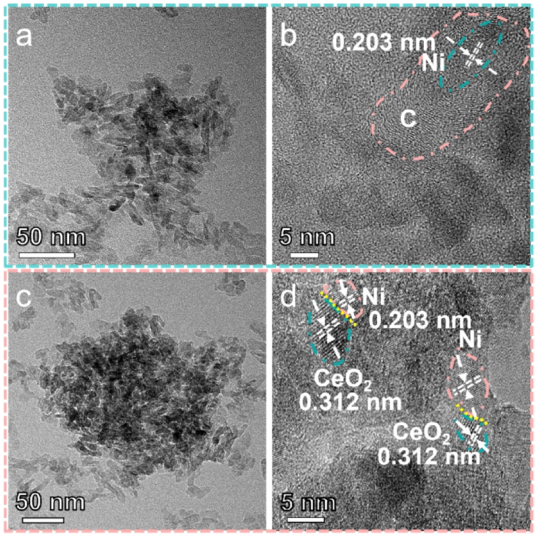

Figure 6. TEM and high resolution TEM images of the used (a, b) Ni/Al_2O_3 and (c, d) Ni/CeO_2-Al_2O_3.

n DISCUSSIONS

SMSI Effect on Ni Catalysts for DRM Reaction. Since Ni/Al_2O_3 and Ni/CeO_2-Al_2O_3 possessed large surface area with almost the same particle size of Ni NPs, it is clearly safe to reveal the relationship between interaction together with interface and their catalytic behaviors during DRM reaction. The interaction between metal and support is crucial for Ni/CeO_2-Al_2O_3 catalyst to achieve stable catalytic performance. This is evidenced by the fact that the control Ni/CeO_2-Al_2O_3 catalyst with weak metal-support interaction (calcinated at 400 °C for 3 h) exhibited poor stability in DRM at 500 °C. The H_2-TPR profile of the control NiO/CeO_2-Al_2O_3 in Figure 7a exhibited three peaks at 550, 680, and 750 °C, which are lower than those of NiO/CeO_2-Al_2O_3. Besides, the surface of the control NiO/CeO_2-Al_2O_3 was composed of NiO and $NiAl_2O_4$ hardly appeared (Figure 7b). The results are originated from the presence of more Ni species weakly interacted with support on the control NiO/CeO_2-Al_2O_3.

The stability test of the control Ni/CeO_2-Al_2O_3 catalyst after reduction is shown in Figure 7c. Obviously, CO_2 and CH_4 conversions on the catalyst declined from 23% to 20% and 14% to 12%, separately. Simultaneously, the H_2/CO ratio decreased from 0.55

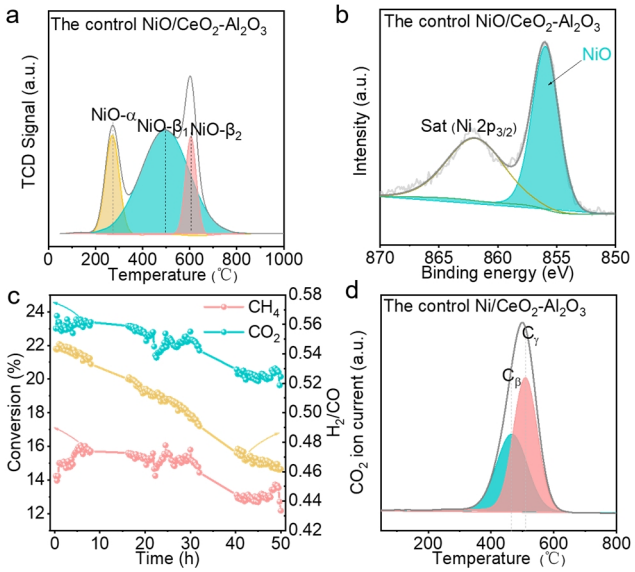

Figure 7. Characterizations and stability test of the control NiO/CeO_2-Al_2O_3 with weak metal-support interaction. (a) H_2-TPR profile and (b) Ni $2p_{3/2}$ XPS spectrum of the control NiO/CeO_2-Al_2O_3. (c) The stability of the control Ni/CeO_2-Al_2O_3 catalyst and (d) O_2-TPO profile of the used catalyst after stability test.

DOI: 10.14102/j.cnki.0254-5861.2022-0113

to 0.45 with 50 h on stream. The amount of deposited carbon on the used catalyst, determined by automatic carbon element analyzer, is 23.4%, corresponding to the coke deposition rate of 0.61 $mg_c\ g_{cat}^{-1}\ h^{-1}$, which is approximately 6 times larger than that of the used Ni/CeO_2-Al_2O_3 with the same reaction condition. The deposited carbon species were originated from the oxidation of C_β and C_γ species, as evidenced by the high burning-off temperature at 470 and 510 °C, respectively (Figure 7d). This is well illustrated by the formation of large amounts of carbon filaments on the used catalyst (Figure S2).

For Ni/CeO_2-Al_2O_3 with the same interface structure but different interaction, the weak metal-support interaction in the control Ni/CeO_2-Al_2O_3 has lower amounts of surface Ce^{3+} species and the ratio of Ce^{3+} to Ce_{total} is 25% (as confirmed by the XPS analysis in Figure S3), which is lower than that of 32% of Ni/CeO_2-Al_2O_3 with strong metal-support interaction. This suggests that metal-support interaction affected the surface amount of Ce^{3+} species, which contributed to the different amounts of surface oxygen vacancies. The higher amount of Ce^{3+} species in Ni/CeO_2-Al_2O_3 with SMSI provided more active oxygen species during DRM, leading to an enhanced gasification rate of carbon species from CH_4 dissociation and an improved catalytic stability with less coke formation. It can also be clearly observed that Ni/CeO_2-Al_2O_3 with SMSI possessed relatively higher activity and lower coke deposition rate in comparison with other catalysts in the literature (Table S3).

Importance of Ni-CeO_2 Interface for CO_2 Activation on Ni/CeO_2-Al_2O_3. In-situ diffuse reflectance infrared Fourier transform spectroscopy (DRIFTS) studies were carried out to monitor the intermediates on Ni/Al_2O_3 and Ni/CeO_2-Al_2O_3 catalysts during DRM at 400 °C (Figure 8). Besides the peaks at 3016/1304, 2300-2400 and 2130/2010 cm^{-1} for CH_4, CO_2 and CO, respectively, three reaction intermediates were observed on the two catalysts.[31] The first type of intermediate was identified as monodentate carbonate species (m-CO_3^{2-}) and bidentate carbonate species (b-CO_3^{2-}), as evidenced by the peaks at 1520-1540 and 1625-1765 cm^{-1}, respectively.[32,33] The second kind of intermediate with the peaks at 1228 and 1440 cm^{-1} was diagnostic of the formation of bicarbonate species (HCO_3^-).[34] The third intermediates, identified from the peaks of 1391 and 1592 cm^{-1}, corresponded to the formation of formate species ($HCOO^-$).[22,35]

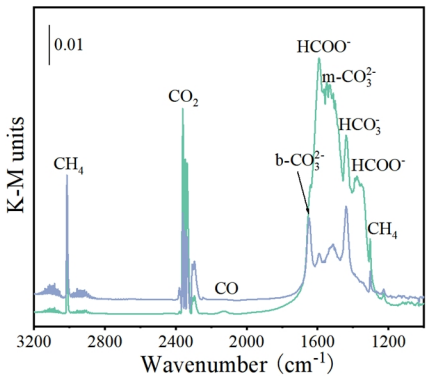

Figure 8. DRIFTS of CH_4 + CO_2 reaction on Ni/Al_2O_3 (blue line) and Ni/CeO_2-Al_2O_3 (green line) at 400 °C.

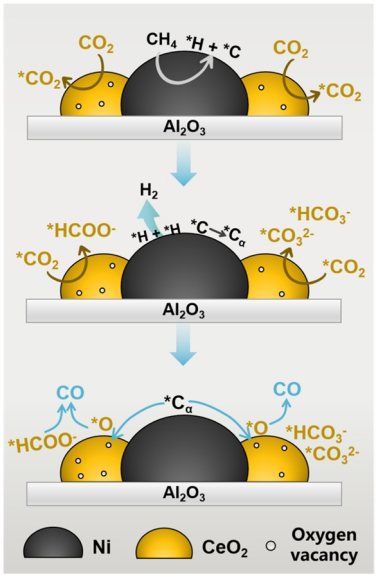

Figure 9. Reaction pathway of Ni/CeO_2-Al_2O_3 catalyst in DRM.

Generally, Ni-based catalysts possessed bi-functional mechanism, where CH_4 and CO_2 separately activated on Ni particles and support.[22,36,37] During the DRIFTs study, carbonate and formate species were detected as intermediates during DRM. The formation of carbonate species was attributed to the reaction of CO_2 + *O.[34,38] The generation of formate species was ascribed to the reaction of $*CO_x$ + *H or CH_x + *O from CO_2 and CH_4 dissociation.[39] Therefore, compared to carbonate species, more formate species indicated the enhanced CO_2 and CH_4 activation in DRM.

It should be noted that carbonate and bicarbonate species were the principal reaction intermediates on Ni/Al_2O_3 and formate species accounted for a minor part. However, the major portion of intermediates for Ni/CeO_2-Al_2O_3 was dominated by the generation of formate species, associated with a relatively small part of carbonate and bicarbonate species. This is well matched with previous work that strong metal-support interaction with abundant interfacial sites promoted surface formate species.[40-42] Therefore, Ni/CeO_2-Al_2O_3 had distinct reaction pathway (as shown in Figure 9) for CO_2 and CH_4 activation and the beneficial effect of major formate species contributed to superior catalytic performance in DRM. Specifically, CH_4 and CO_2 activation occurred separately on Ni and support of Ni/CeO_2-Al_2O_3, which produced carbon atoms with hydrogen atoms (as evidenced from O_2-TPO results) and carbonate, bicarbonate with formate species (as confirmed by DRIFTS analysis), respectively. Owing to strong metal-support interaction and tailored interface in Ni/CeO_2-Al_2O_3, more active interfacial sites accelerated the conversion of carbon atoms and promoted the generation of more formate species as key intermediates (with less carbonate species), leading to a distinct reaction pathway and improved catalytic performance in DRM.

n CONCLUSIONS

In the present work, we employed an improved evaporation-induced self-assembly method to design Ni/Al_2O_3 and Ni/CeO_2-Al_2O_3 catalysts by SMSI effect but distinct interface structure. The

DOI: 10.14102/j.cnki.0254-5861.2022-0113

only difference of the resultant catalysts is the interface structure between Ni metal and CeO_2 or Al_2O_3 support. Compared to Ni/Al_2O_3, Ni particles over Ni/CeO_2-Al_2O_3 were closely interacted and intimately contacted with CeO_2, leading to the formation of interface structure between metal and support. This unique interface structure renders Ni/CeO_2-Al_2O_3 with higher catalytic activity and better stability relative to Ni/Al_2O_3. Less carbonaceous species with higher reactivity were formed on the used Ni/CeO_2-Al_2O_3, whereas more coke deposition was observed on the used Ni/Al_2O_3. However, the control Ni/CeO_2-Al_2O_3 with weak metal-support interaction possessed inferior performance and large amounts of coke deposition. The same SMSI effect with different interface structure altered the reaction intermediates during DRM, where carbonate and bicarbonate species were produced on Ni/Al_2O_3, but majority of formate species with carbonate and bicarbonate species were obtained on Ni/CeO_2-Al_2O_3.

n EXPERIMENTAL

Preparation of the Catalysts. In a typical synthesis, 2.4 g of pseudo-boehmite powder (SINOPEC Dalian Research Institute of Petroleum and Petrochemicals) was dispersed in 30 mL of distilled water, and then 0.55 mL concentrated nitric acid (Sinopharm Chemical Reagent Co., Ltd) was dropped into the above solution with a $[H^+]$ to $[Al^{3+}]$ ratio of 0.2. Next, the mixture was treated under microwave irradiation at 70 °C for 1 h under continuous stirring to produce white semi-transparent alumina gel. Meanwhile, 5 g of triblock copolymer Pluronic P123 (Sigma Aldrich) together with 0.79 g of $Ce(NO_3)_3{\cdot}6H_2O$ and 1.26 g of $Ni(NO_3)_2{\cdot}6H_2O$ (Sinopharm Chemical Reagent Co., Ltd) was dissolved into 40 mL of ethanol (100%), and then stirred for 4 h. The alumina gel was added to the solution with stirring for another 4 h. Afterwards, the sample was placed in an oven to evaporate the solvent firstly at 60 °C for 48 h, and then at 100 °C for another 48 h. Finally, the solid powder was calcined at 600 °C with a heating rate of 1 °C min^{-1} under air for 4 h, and the product was denoted as NiO/CeO_2-Al_2O_3.

NiO/Al_2O_3 was prepared with the same method, except the only addition of 1.12 g of $Ni(NO_3)_2{\cdot}6H_2O$ to the ethanol in the second step. Ni/Al_2O_3 and Ni/CeO_2-Al_2O_3 were obtained by reducing with H_2 at 550 °C for 2 h.

Characterizations. The Ni and/or Ce loading on NiO/Al_2O_3 or NiO/CeO_2-Al_2O_3 was determined by inductively coupling plasma-atomic emission spectrometry (ICP-AES) on a Thermo iCAP 6300 spectrometer. The component structure of the samples was studied by powder X-ray diffraction (XRD) measurements on a Rigaku D/Max-2500 diffractometer with a scanning region from 10° to 80° at a scanning speed of 2 ° min^{-1}. The texture properties of the samples were investigated by N_2 adsorption-desorption experiment at -196 °C on a NOVA1200e analyzer (Quantachrome), and the samples were pretreated under vacuum at 300 °C for 3 h before the test. Surface structure of the samples was studied by X-ray photoelectron spectroscopy (XPS) on a Thermo SCIENTIFIC ESCALAB 250XI spectrometer. The binding energies of Ni and Ce were calibrated with C 1s peak at 284.8 eV. The morphological structure of the samples was depicted by scanning electron microscopy (SEM) on a JEOL JSE-7100F apparatus and transmission electron microscope (TEM) with energy-dispersive X-ray spectroscopy (EDX) on an FEI Tecnai G20 instrument operated at 200 kV.

The reductive behavior of the samples was investigated by H_2 temperature programmed reduction (H_2-TPR) measurement on a Micromeritics AutoChem II 2920 Chemisorption instrument. 0.1 g of the sample was firstly purged under Ar (30 mL min^{-1}) at 300 °C for 1 h, and then cooled down to 30 °C. Next, 10% H_2/He (30 mL min^{-1}) was switched into the reactor and the temperature was increased to 1000 °C at a heating rate of 10 °C min^{-1}. The signal of H_2 consumption was recorded on a TCD detector. The surface area of the active nickel was measured by pulse H_2 chemisorption experiment on the same equipment. 0.1 g of the sample was reduced at 550 °C under 10% H_2/He (30 mL min^{-1}) for 2 h, then the temperature was declined to 50 °C under Ar. Next, 100 μL of 10% H_2/He was injected into the sample until it was saturated.

The amount and property of coke deposition on the used samples were analyzed by oxidation under air from 50 to 800 °C on a thermal analyzer (TG, Setaram SETSYS, TGA) coupled with mass spectrometer (MS, Hiden HPR20 QIC R&D).

The reaction intermediates and pathways on the catalysts during dry reforming of methane were monitored by in-situ diffuse reflectance infrared Fourier transform spectroscopy (DRIFTS) on an FT-IR spectrometer (Bruker Vertex 70) equipped with a liquid nitrogen cooled Mercury-Cadmium-Tellurium (MCT) detector and a diffuse reflectance accessory (Praying Mantis, Pike). The sample was firstly reduced ex-situ at 550 °C for 2 h under H_2 in a tube furnace. Afterwards, the powder sample was transferred into a crucible in the reaction cell and then reduced in-situ at 550 °C under 5% H_2/He (20 mL min^{-1}) for 2 h. Next, the sample was purged with He (20 mL min^{-1}) for 30 min and then cooled down to 400 °C. Meanwhile, a background spectrum was recorded under He. Finally, 5% CH_4/He (10 mL min^{-1}) and 5% CO_2/He (10 mL min^{-1}) were introduced into the reaction cell and IR spectra with background spectrum subtracted (resolution of 4 cm^{-1} with 128 scans) on the reduced catalysts during the reaction were collected at 400 °C.

Catalyst Evaluation. Dry reforming of methane (DRM) reaction was performed on a vertical fixed-bed reactor (10 mm of inner diameter and 300 mm of length) in a temperature range of 400 to 700 °C under atmospheric pressure. Typically, 50 mg of catalyst (20-40 mesh) diluted with 1 g of quartz was placed into the reactor. The catalyst was reduced at 550 °C under a H_2 flow (50 mL min^{-1}) for 2 h and then the temperature was decreased to 400 °C in an Ar flow (50 mL min^{-1}). Finally, a feed gas of CH_4/CO_2 (1:1) flow (20 mL min^{-1}) was introduced into the reactor for DRM. The emission was monitored by an online gas chromatograph (GC, Agilent 7820) equipped with a thermal conductivity detector (TCD) with a TDX-01 column (2 m). An ice trap was used to condense water during the reaction before the GC. The stability test of the catalyst was performed at 500 °C for 50 h with a feed gas of CH_4/CO_2/He (1:1) flow (20 mL min^{-1}).

X_{CH4} and X_{CO2} and H_2/CO ratio were calculated based on the following equations:

$$X_{CH_4} = \frac{F_{CH_4,in} - F_{CH_4,out}}{F_{CH_4,in}} \times 100\%$$

Chin. J. Struct. Chem. **2022**, 41, 2212007-2212014
DOI: 10.14102/j.cnki.0254-5861.2022-0113

$$X_{CO_2} = \frac{F_{CO_2,in} - F_{CO_2,out}}{F_{CO_2,in}} \times 100\%$$

$$\frac{H_2}{CO} = \frac{F_{H_2}}{F_{CO}}$$

where $F_{i,in}$ and $F_{i,out}$ represent the molar flow rate of component *i* of the inlet and outlet, respectively.

n ACKNOWLEDGEMENTS

The authors acknowledge the National Natural Science Foundation of China (Nos. 22108189, 21878203), the Program for the Top Young and Middle-Aged Innovative Talents of Higher Learning Institutions of Shanxi, and the financial support by Shanxi-Zheda Institute of Advanced Materials and Chemical Engineering (2021SX-TD005).

n AUTHOR INFORMATION

Corresponding author. Email: yanxiaoliang@tyut.edu.cn

n COMPETING INTERESTS

The authors declare no competing interests.

n ADDITIONAL INFORMATION

Supplementary information is available for this paper at http://manu30.magtech.com.cn/jghx/EN/10.14102/j.cnki.0254-5861.2022-0113

For submission: https://www.editorialmanager.com/cjschem

n REFERENCES

(1) Diao, Y. N.; Zhang, X.; Liu, Y.; Chen, B. B.; Wu, G. H.; Shi, C. Plasma-assisted dry reforming of methane over Mo_2C-Ni/Al_2O_3 catalysts: effects of β-Mo_2C promoter. *Appl. Catal. B Environ.* **2022**, 301, 120779.

(2) Guo, Y.; Li, Y. F.; Ning, Y. X.; Liu, Q. K.; Tian, L.; Zhang, R. D.; Fu, Q.; Wang, Z. J. CO_2 reforming of methane over a highly dispersed Ni/Mg-Al-O catalyst prepared by a facile and green method. *Ind. Chem. Eng. Res*. **2020**, 59, 15506-15514.

(3) Zhang, T. T.; Liu, Z. X.; Zhu, Y. A.; Liu, Z. C.; Sui, Z. J.; Zhu, K. K.; Zhou, X. G. Dry reforming of methane on Ni-Fe-MgO catalysts: influence of Fe on carbon-resistant property and kinetics. *Appl. Catal. B Environ.* **2020**, 264, 118497.

(4) Song, Y.; Ozdemir, E.; Ramesh, S.; Adishev, A.; Subramanian, S.; Harale, A.; Albuali, M.; Fadhel, B. A.; Jamal, A.; Moon, D.; Choi, S. H.; Yavuz, C. T. Dry reforming of methane by stable Ni-Mo nanocatalysts on single-crystalline MgO. *Science* **2020**, 367, 777-781.

(5) Liu, C. J.; Ye, J. Y.; Jiang, J. J.; Pan, Y. X. Progresses in the preparation of coke resistant Ni-based catalyst for steam and CO_2 reforming of methane. *ChemCatChem* **2011**, 3, 529-541.

(6) Chen, S. Y.; Zaffran, J.; Yang, B. Descriptor design in the computational screening of Ni-based catalysts with balanced activity and stability for dry reforming of methane reaction. *ACS Catal.* **2020**, 10, 3074-3083.

(7) Huang, Y. L.; Li, X. D. Zhang, Q.; Vinokurov, V. A.; Huang, W. Carbon deposition behaviors in dry reforming of CH_4 at elevated pressures over Ni/MoCeZr/$MgAl_2O_4$-MgO catalysts. *Fuel* **2022**, 310, 122449.

(8) Azancot, L.; Bobadilla, L. F.; Centeno, M. A.; Odriozola, J. A. IR spectroscopic insights into the coking-resistance effect of potassium on nickel-based catalyst during dry reforming of methane. *Appl. Catal. B Environ.* **2021**, 285, 119822.

(9) Liu, Z. Y.; Grinter, D. C.; Lustemberg, P. G.; Nguyen-Phan, T. D.; Zhou, Y. H.; Luo, S.; Waluyo, I.; Crumlin, E. J.; Stacchiola, D. J.; Zhou, J.; Carrasco, J.; Busnengo, H. F.; Ganduglia-Pirovano, M. V.; Senanayake, S. D.; Rodriguez, J. A. Dry reforming of methane on a highly-active Ni-CeO_2 catalyst: effects of metal-support interactions on C-H bond breaking. *Angew. Chem. Int. Ed.* **2016**, 55, 7455-7459.

(10) Akri, M.; Zhao, S.; Li, X. Y.; Zang, K. T.; Lee, A. F.; Isaacs, M. A.; Xi, W.; Gangarajula, Y.; Luo, J.; Ren, Y. J.; Cui, Y. T.; Li, L.; Su, Y.; Pan, X. L.; Wen, W.; Pan, Y.; Wilson, K.; Li, L.; Qiao, B. T.; Ishii, H.; Liao, Y. F.; Wang, A. Q.; Wang, X. D.; Zhang, T. Atomically dispersed nickel as coke-resistant active sites for methane dry reforming. *Nat. Commun.* **2019**, 10, 5181.

(11) Ewbank, J. L.; Kovarik, L.; Diallo, F. Z.; Sivers, C. Effect of metal-support interactions in Ni/Al_2O_3 catalysts with low metal loading for methane dry reforming. *Appl. Catal. A Gen.* **2015**, 494, 57-67.

(12) Yang, B.; Deng, J.; Li, H. R.; Yan, T. T.; Zhang, J. P.; Zhang, D. S. Coking-resistant dry reforming of methane over Ni/gamma-Al_2O_3 catalysts by rationally steering metal-support interaction. *iScience* **2021**, 24, 102747.

(13) Zhou, L.; Li, L. D.; Wei, N. N.; Li, J.; Basset, J. M. Effect of $NiAl_2O_4$ formation on Ni/Al_2O_3 stability during dry reforming of methane. *ChemCatChem* **2015**, 7, 2508-2516.

(14) Zhang, S. S.; Ying, M.; Yu, J.; Zhan, W. C.; Wang, L.; Guo, Y.; Guo, Y. L. $Ni_xAl_1O_2$-delta mesoporous catalysts for dry reforming of methane: the special role of $NiAl_2O_4$ spinel phase and its reaction mechanism. *Appl. Catal. B Environ.* **2021**, 291, 120074.

(15) Li, K.; Pei, C. L.; Li, X. Y.; Chen, S.; Zhang, X. H.; Liu, R.; Gong, J. L. Dry reforming of methane over $La_2O_2CO_3$-modified Ni/Al_2O_3 catalysts with moderate metal support interaction. *Appl. Catal. B Environ.* **2020**, 264, 118448.

(16) Stroud, T.; Smith, T. J.; Le, S. E.; Santos, J. L.; Centeno, M. A.; Arellano-Garcia, H.; Odriozola, J. A.; Reina, T. R. Chemical CO_2 recycling via dry and bi reforming of methane using Ni-Sn/Al_2O_3 and Ni-Sn/CeO_2-Al_2O_3 catalysts. *Appl. Catal. B Environ.* **2018**, 224, 125-135.

(17) Wang, S. B.; Lu, M. Role of CeO_2 in Ni/CeO_2-Al_2O_3 catalysts for carbon dioxide reforming of methane. *Appl. Catal. B Environ.* **1998**, 19, 267-277.

(18) Peng, W. X.; Wang, L. S.; Mirzaee, M.; Ahmadi, H.; Esfahani, M. J.; Fremaux, S. Hydrogen and syngas production by catalytic biomass gasification. *Energy Convers. Manage.* **2017**, 135, 270-273.

(19) Biset-Peiró, M.; Guilera, J.; Zhang, T.; Arbiol, J.; Andreu, T. On the role of ceria in Ni-Al_2O_3 catalyst for CO_2 plasma methanation. *Appl. Catal. A Gen.* **2019**, 575, 223-229.

(20) Luisetto, I.; Tuti, S.; Battocchio, C.; Lo Mastro, S.; Sodo, A. Ni/CeO_2-Al_2O_3 catalysts for the dry reforming of methane: the effect of $CeAlO_3$ content and nickel crystallite size on catalytic activity and coke resistance. *Appl. Catal. A Gen.* **2015**, 500, 12-22.

(21) Ahmed, W.; Awadallah, A. E.; Aboul-Enein, A. A. Ni/CeO_2-Al_2O_3 catalysts for methane thermo-catalytic decomposition to CO_x-free H_2 production. *Int. J. Hydrogen Energy* **2016**, 41, 18484-18493.

(22) Anita, H.; Miklós, N.; Andrea, B.; Boglárka, M.; György, S.; Giuseppe, P.; Leonarda, F. L.; Anna, M. V.; ValeriaLa, P. Strong impact of indium promoter on Ni/Al_2O_3 and Ni/CeO_2-Al_2O_3 catalysts used in dry reforming of methane. *Appl. Catal. A Gen.* **2021**, 621, 118174.

(23) Song, Z. W.; Wang, Q. Q.; Guo, C.; Li, S.; Yan, W. J.; Jiao, W. Y.; Qiu, L.; Yan, X. L.; Li, R. F. Improved effect of Fe on the stable NiFe/Al_2O_3 catalyst in low-temperature dry reforming of methane. *Ind. Eng. Chem. Res.* **2020**, 59, 17250-17258.

DOI: 10.14102/j.cnki.0254-5861.2022-0113

(24) Meng, F. H.; Li, X.; Li, M. H.; Cui, X. X.; Li, Z. Catalytic performance of CO methanation over La-promoted Ni/Al_2O_3 catalyst in a slurry-bed reactor. *Chem. Eng. J.* **2016**, 313, 1548-1555.

(25) Rynkowski, J. M.; Paryjczak, T.; Lenik, M. On the nature of oxidic nickel phases in NiO/γ-Al_2O_3 catalysts. *Appl. Catal. A Gen.* **1993**, 106, 73-82.

(26) Ai, H. M.; Yang, H. Y.; Liu, Q.; Zhao, G. M.; Yang, J.; Gu, F. N. ZrO_2-modified Ni/$LaAl_{11}O_{18}$ catalyst for CO methanation: effects of catalyst structure on catalytic performance. *Chin. J. Catal.* **2018**, 39, 297-308.

(27) Tan, M.; Wang, X.; Wang, X.; Zou, X.; Ding, W.; Lu, X. Influence of calcination temperature on textural and structural properties, reducibility, and catalytic behavior of mesoporous γ-alumina-supported Ni-Mg oxides by one-pot template-free route. *J. Catal.* **2015**, 329, 151-166.

(28) Yan, X. L.; Zhao, B. R.; Liu, Y.; Li, Y. N. Dielectric barrier discharge plasma for preparation of Ni-based catalysts with enhanced coke resistance: current status and perspective. *Catal. Today* **2015**, 256, 29-40.

(29) Al-Fatesh, A. S.; Naeem, M. A.; Fakeeha, A. H.; Abasaeed, A. E. Role of La_2O_3 as promoter and support in Ni/γ-Al_2O_3 catalysts for dry reforming of methane. *Chin. J. Chem. Eng.* **2014**, 22, 28-37.

(30) McCarty, J. G.; Wise, H. Hydrogenation of surface carbon on alumina-supported nickel. *J. Catal.* **1979**, 57, 406-416.

(31) Vogt, C.; Groeneveld, E.; Kamsma, G.; Nachtegaal, M.; Lu, L.; Kiely, C. J.; Berben, P. H.; Meirer, F.; Weckhuysen, B. M. Unravelling structure sensitivity in CO_2 hydrogenation over nickel. *Nat. Catal.* **2018**, 1, 127-134.

(32) Pan, Y.; Liu C. J.; Ge, Q. Adsorption and protonation of CO_2 on partially hydroxylated γ-Al_2O_3 surfaces: a density functional theory study. *Langmuir* **2008**, 24, 12410-12419.

(33) Busca, G.; Lorenzelli, V. Infrared spectroscopic identification of species arising from reactive adsorption of carbon oxides on metal oxide surfaces. *Mater. Chem.* **1982**, 7, 89-126.

(34) Wang, X.; Hong, Y. C.; Shi, H.; Szanyi, J. Kinetic modeling and transient DRIFTS-MS studies of CO_2 methanation over Ru/Al_2O_3 catalysts. *J. Catal.* **2016**, 343, 185-195.

(35) Alarcon, A.; Guilera, J.; Soto, R.; Andreu, T. Higher tolerance to sulfur poisoning in CO_2 methanation by the presence of CeO_2. *Appl. Catal. B Environ.* **2020**, 263, 118346.

(36) Zhang, X. Y.; Deng, J.; Pupucevski, M.; Impeng, S.; Yang, B.; Chen, G. R.; Kuboon, S.; Zhong, Q. D.; Faungnawakij, K.; Zheng, L. R.; Wu, G.; Zhang, D. S. High-performance binary Mo-Ni catalysts for efficient carbon removal during carbon dioxide reforming of methane. *ACS Catal.* **2021**, 11, 12087-12095.

(37) Shi, L.; Yang, G. H.; Tao, K.; Yoneyama, Y.; Tan, Y. S.; Tsubaki, N. An introduction of CO_2 conversion by dry reforming with methane and new route of low-temperature methanol synthesis. *Acc. Chem. Res.* **2013**, 46, 1838-1847.

(38) Szanyi, J.; Kwak, J. H. Dissecting the steps of CO_2 reduction: 2. The interaction of CO and CO_2 with Pd/gamma-Al_2O_3: an in situ FTIR study. *Phys. Chem. Chem. Phys.* **2014**, 16, 15126-15138.

(39) Ni, J.; Chen, L. W.; Lin, J. Y.; Kawi, S. Carbon deposition on borated alumina supported nano-sized Ni catalysts for dry reforming of CH_4. *Nano Energy* **2012**, 1, 674-686.

(40) Ferreira-Aparicio, P.; Fernandez-Garcia, M.; Guerrero-Ruiz, A.; Rodríguez-Ramos, I. Evaluation of the role of the metal-support interfacial centers in the dry reforming of methane on alumina-supported rhodium catalysts. *J. Catal.* **2000**, 190, 296-308.

(41) Luo, J. Z.; Yu, Z. L.; Ng, C. F.; Au, C. T. CO_2/CH_4 reforming over Ni-La_2O_3/5A: an investigation on carbon deposition and reaction steps. *J. Catal.* **2000**, 194, 198-210.

(42) Yan, X. L.; Hu, T.; Liu, P.; Li, S.; Zhao, B. R.; Zhang, Q.; Jiao, W. Y.; Chen, S.; Wang, P. F.; Lu, J. J. Highly efficient and stable Ni/CeO_2-SiO_2 catalyst for dry reforming of methane: effect of interfacial structure of Ni/CeO_2 on SiO_2. *Appl. Catal. B Environ.* **2019**, 246, 221-231.

Received: May 7, 2022
Accepted: August 1, 2022
Published online: August 6, 2022
Published: December 2, 2022

DOI: 10.14102/j.cnki.0254-5861.2022-0113